AIAA JOURNAL
Vol. 36, No. 7, July 1998

Numerical Simulation of High-Speed Civil Transport Inlet Operability with Angle of Attack

Ge-Cheng Zha,* Doyle Knight,† and Donald Smith‡
Rutgers University, Piscataway, New Jersey 08854
and
Martin Haas§
United Technologies Research Center, East Hartford, Connecticut 06180

A high-speed civil transport inlet at Mach 2 and angle of attack is simulated by using a three-dimensional Navier–Stokes solver with the Baldwin–Lomax algebraic turbulence model. An extrapolation uniform mass bleed boundary condition for the slot bleed is successfully employed. At zero angle of attack and critical operation, the computational pressure distribution agrees well with the experiment. The location and intensity of the terminal shock and the total pressure recovery are accurately computed. The predicted steady-state distortion deviates from the experiment. The computed maximum angle of attack that the inlet can sustain before unstart is in good agreement with the experiment. Mesh refinement results are presented.

Nomenclature

H	= total radial distance between the wall of centerbody and cowl
h	= radial distance from centerbody wall
M_∞	= freestream Mach number
$P_{t\infty}$	= freestream total pressure
R_c	= radius at cowl leading edge
$T_{t\infty}$	= freestream total temperature
α	= angle of attack
Δr	= grid point interval in radial direction
Δr_1^+	= $(\Delta r_1 u_\tau)/\nu$
Δx	= grid point interval in axial direction
δ	= boundary-layer thickness on centerbody

I. Introduction

THE critical technologies required to develop a high-speed civil transport (HSCT) are being investigated in the United States and Europe. A high-performance HSCT propulsion system and airframe are vital for competition in the global HSCT market.[1,2] The supersonic flight regime of the HSCT results in issues that are not present for its subsonic counterpart. As an important component of the HSCT propulsion system, the HSCT inlet needs to work with high efficiency and a wide stability margin.

Inlet unstart at the cruise condition is an extremely important issue in the design of an HSCT inlet. For flight speeds over Mach 2, mixed-compression inlets offer the capability to operate efficiently with low drag over the entire flight range. For high cruise efficiency, the mixed compression inlet is designed to operate with a terminal shock just downstream of the throat to maintain high total pressure recovery with maximum mass flow. For such a flow condition, the inlet is said to remain started. However, the terminal shock location is very sensitive to disturbances and can be pushed out of the inlet, causing the inlet to unstart. An inlet unstart would result in transient forces on the aircraft, which would affect passenger comfort and safety and which may also cause engine surge. The range of operating conditions, e.g., Mach number, angle of attack, etc., wherein the inlet remains started, is known as the operability of the inlet.

Disturbances that may cause inlet unstart could originate through either a variation of upstream flight conditions or a corrected weight flow required by the compressor. To increase the inlet control operability, boundary-layer bleed is usually employed in the region of the throat to resist the disturbance. The design of boundary-layer bleed, such as the bleed location and bleed mass flow rate, is crucial to provide an HSCT inlet with high efficiency, broad stability margin, and low drag. To design high-performance boundary-layer bleed, wind-tunnel tests are necessary. However, with more and more powerful computers, to reduce the design cycle and costs, computational fluid dynamics (CFD) is now usually used to guide the design before the final test.

Nevertheless, using CFD to accurately simulate the HSCT inlet flow with boundary-layer bleed is very challenging. For the NASA variable diameter centerbody (VDC) inlet, which is studied in this paper, Saunders and Keith[3] did the first CFD simulation with zero angle of attack by using an axisymmetric Navier–Stokes solver. They used two different types of bleed boundary conditions. One was to specify the tangential and normal velocity profiles across the bleed slot region,[4] and the other was to use constant pressure across the bleed region and adjust the bleed mass flow rate to the required one incorporated in the PARC code.[5] Saunders and Keith[3] indicated significant difficulties in computing the critical flow. They obtained the critical flow with either the back pressure at the inlet outflow boundary reduced by about 18% from the experimental value or the cowl translated by 3%. The computational difficulties were mainly attributed to the bleed boundary conditions used. Slater et al.[6] used boundary conditions similar to the constant pressure boundary condition of the PARC code and computed the same inlet at zero angle of attack. The shock location was significantly displaced from the experimental position when the experimental back pressure of the critical flow was imposed.

For the operability of high-speed, mixed-compression inlets, various numerical studies have been carried out focusing on different subjects. Mayer and Paynter[7,8] used an Euler solver and simulated the inlet operability due to the variation of freestream variables such as temperature, velocity, and pressure. Slater et al.[6] and Slater[9] simulated the unstart/restart due to the freestream disturbance with moving geometry. Neaves and McRae[10] used the dynamic solution-adaptive grid algorithm of Benson and McRae[11] and simulated the two- and three-dimensional inlet unstart due to the freestream and compressor face perturbations. Goble et al.[12] used a

Received Feb. 28, 1997; revision received March 16, 1998; accepted for publication March 30, 1998.

*Research Associate, Department of Mechanical and Aerospace Engineering, Center for Computational Design; currently Visiting Scientist, CFD Research Section, U.S. Air Force Research Laboratory (AFRL/VAAC), Building 450, 2645 Fifth Street, Suite 7, Dayton, OH 45433-7913. Member AIAA.

†Professor, Department of Mechanical and Aerospace Engineering, Center for Computational Design, 98 Brett Road. Associate Fellow AIAA.

‡Research Associate Professor, Department of Computer Sciences, Center for Computational Design.

§Senior Research Engineer, Advanced Propulsion Department. Member AIAA.

three-dimensional Euler code to simulate the unsteady flow of the F-22 inlet with the hammer shock from the engine face. Miller and Smith[13] conducted a Navier–Stokes simulation of two-dimensional high-speed inlet unstart due to the back pressure disturbance. These studies made contributions from different aspects to investigate the high-speed inlet operability with boundary-layer bleed. However, most of the results did not have experiments with which to be compared and are not quantitative. Some comparisons with experiments were given in Ref. 6, but the shock location and profile largely deviated from the experiment at critical operation under the experimental back pressure. Their results were, thus, still at the qualitative level. These studies were all at zero angle of attack. Hence, for some of the cases, the computation benefited from the axisymmetry of the flowfield to save CPU time.

For the numerical studies on high-speed inlet operability at angle of attack with boundary-layer bleed, no work has been reported. Vadyak et al.[14] made the first computation of the flowfield of a mixed-compression inlet with angle of attack using the method of characteristics with shock fitting. Because of the limitations of the method of characteristics, they did not take into account the wall boundary layer and boundary-layer bleed. Thus, they[14] were not able to predict the angle of attack that would induce inlet unstart. Howlett and Hunter[15] computed a three-dimensional external compression inlet at angle of attack. The unstart was not a problem in their work, and there was no boundary-layer bleed in that inlet.

The purpose of the present work is to use CFD to predict the maximum angle of attack that the NASA VDC inlet can sustain before it unstarts. This work is the first computational effort to study the unstart of a mixed-compression inlet with boundary-layer bleed at angle of attack. Accurate simulation of HSCT inlet operability due to angle of attack is very important to achieve a design of HSCT inlet with high efficiency and wide stability margin.[16]

II. Inlet

The inlet studied is the NASA VDC inlet designed and tested at NASA Lewis Research Center in 1975, as shown in Fig. 1 (Refs. 17–19). It is a bicone, mixed-compression inlet with design cruise Mach number 2.5. A two-cone spike was used to provide the maximum external compression compatible with high total pressure recovery and relatively low cowl drag. To vary the contraction ratio for a flight inlet, the angle of the second cone could vary, and at its lowest position it would blend into the first-cone contours so as to provide a single-cone centerbody. This structure provides 45% of the supersonic area internal contraction for a design Mach number of 2.5. The inlet was designed such that the cowl–lip oblique shock and the isentropic compression from the cowl were nearly focused on the inlet's centerbody. A centerbody bleed slot was provided over this compression region for boundary-layer control just ahead of the inlet throat. The inlet was tested at Mach numbers of 2.5 and 2. At Mach 2.5 at the critical operation, the maximum total pressure recovery with only 0.02 centerbody bleed mass flow ratio and no cowl bleed was 0.906. The bleed mass flow ratio is the ratio of bleed mass flow rate to the captured mass flow rate of the inlet. At Mach 2, the inlet total pressure recovery was 0.938 with only 0.013 centerbody bleed mass flow ratio at critical operation. For both Mach numbers and geometries, the experiment provided data for the maximum angles of attack before inlet unstart is induced. In this study, we examine the Mach 2 case, which had a sealed downstream bypass door (and, hence, no bleed in the subsonic diffuser) so that the computation could be more easily implemented. For the Mach 2 geometry, the initial cone angle was 12.5 deg, and the second cone angle was 14.5 deg.

III. Procedures Determining the Angle of Attack

In the experiment, the procedure used to obtain the maximum angle of attack at critical inlet operation, from Ref. 17, is as follows:

> (1) The inlet was set at the critical operating point for 0 deg angle of attack, and (2) the model angle of attack was increased until an unstart occurred. The inlet was restarted, and data were then recorded for an angle slightly less than the unstart angle of attack.

During the process varying angle of attack, the inlet mass flow plug had constant area, and the corrected mass flow rate was unchanged.

In our computation, we use the following procedure, which is similar to the experimental procedure. 1) At 0-deg angle of attack, a bisection method[20] is used to search the inlet exit back pressure, which positions the terminal shock at the same location as it was at the experimental critical operation. The computational critical operation is, therefore, set up. 2) The back pressure is then held constant, and the angle of attack is gradually increased. A bisection method is also used to search the interval uncertainty of the maximum angle of attack that keeps the inlet started.

The described computational procedure to search the maximum angle of attack is considered to be consistent with the experimental procedure. The reasons are the following. 1) The inlet geometry and freestream parameters used are the same as those in the experiment, which gives the same Reynolds number and Mach number. 2) In the computation, the corrected mass flow rate is virtually constant. The ratio of the computed corrected mass flow rates at zero angle of attack and at the maximum angle of attack is 0.999.

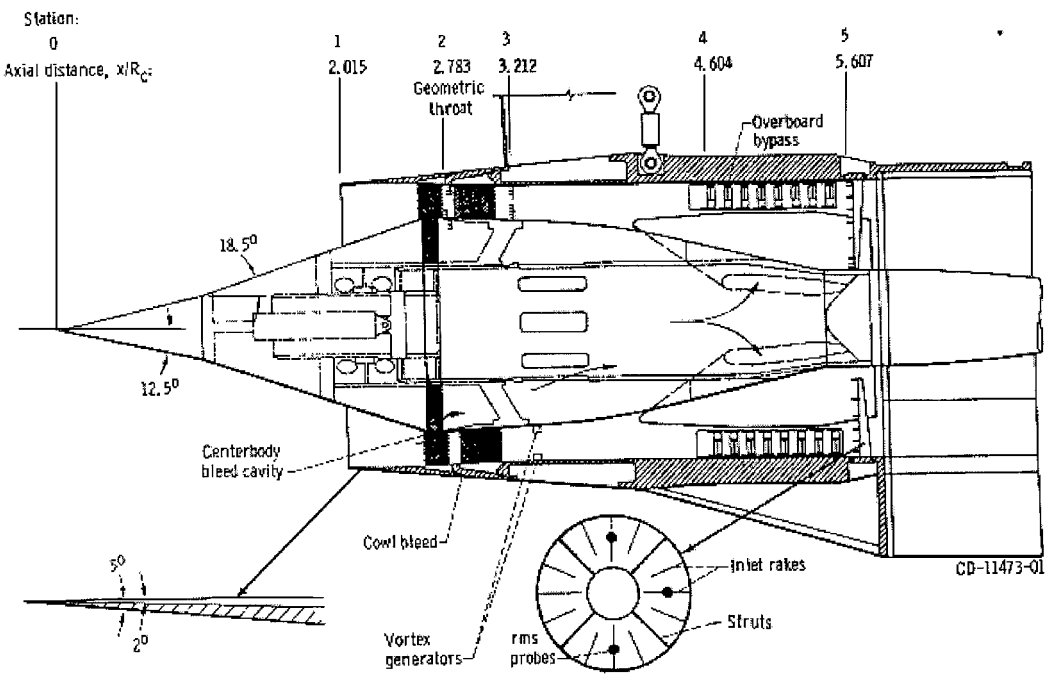

Fig. 1 NASA VDC inlet cross section (from Ref. 17).

IV. Numerical Procedures

A. Flow Solver and Mesh

To simulate the HSCT inlet operability, accurate prediction of the following physical phenomena is critical: 1) wall boundary-layer development, 2) boundary-layer bleed, 3) shock quality (shock intensity and propagation speed), and 4) shock wave/turbulent boundary-layer interaction. To meet these physical needs, the following numerical procedure and boundary conditions were used.

The three-dimensional, steady-state solution of the inlet flowfield was obtained using the GASP code,[21] which solves the Reynolds-averaged three-dimensional compressible time-dependent Navier–Stokes equations. When the inlet remains started, the flowfield is considered stable. Because the purpose of this paper is to predict the maximum angle of attack that keeps the inlet started, we, therefore, employed the techniques for achieving a steady-state solution in the GASP code.

The Baldwin–Lomax algebraic turbulence model was used to simulate the effects of turbulence. According to the experiment, there was no separation as long as the inlet remained started. Therefore, we expect that the Baldwin–Lomax turbulence model will perform well to predict the maximum angle of attack before inlet unstart is induced. Mizukami and Saunders[22] compared the performance of the turbulence models of Baldwin–Lomax, Baldwin–Barth, and the k–ϵ model. They observed that the inlet flows predicted were fairly insensitive to the different turbulence models used. Once the terminal shock wave moves out of the bleed region, it will continue to move upstream, causing separation on the shoulder of the inlet, and eventually bring the inlet to unstart. In this case, although the Baldwin–Lomax model may not predict the details of the flow separation accurately, it has little influence on the objective of this paper, which is to predict the maximum angle of attack that keeps the inlet started. The Baldwin–Lomax algebraic turbulence model also gives us an important advantage that this model is CPU time efficient due to its simplicity, with no additional differential equation to be solved. This advantage is significant because the computation in this work is CPU time intensive.

The Van Leer scheme was used to evaluate the inviscid flux. The Roe scheme was tested first, was able to compute only the axisymmetric flow, and failed in three-dimensional flow due to an anomalous solution.[23] The Van Leer scheme was satisfactory for all flows. The other important merit of the Van Leer scheme was that the allowable Courant–Friedrichs–Lewy number was 18, which was about five times higher than that of the Roe scheme. This was important because multiple-flowfield simulations were required at different angles of attack and back pressures. The third-order MUCSL-type differencing with min–mod limiter was used to evaluate the inviscid interface flux. Second-order central differencing is used to evaluate the viscous terms. The overall accuracy order of the converged solution is, therefore, second order. The time integration method was the hybrid approximate factorization (AF)/relaxation, which solved the implicit operator by using an AF in the spanwise plane and relaxation sweeping in the streamwise direction. One streamwise sweep per time step and no inner iterations were used. The initial flowfield was generated assuming uniform freestream flow with the mesh sequencing technique.

Figure 2 is the three-dimensional mesh used for the NASA VDC inlet[17] with 201 points in the streamwise direction, 31 points in the circumferential direction, and 81 points in the radial direction. The narrow band before the inlet throat with the dense mesh in the streamwise direction is the boundary-layer bleed region. Tables 1 and 2 show the flow conditions and mesh conditions, respectively.

The axisymmetric baseline case has the same mesh size as that in a plane of the baseline three-dimensional mesh, as shown in Table 2. One of the purposes of the axisymmetric computation is to verify if the circumferential mesh size is sufficient for the three-dimensional computation. Because the computational cells are represented by straight line segments, the mesh point distribution in the circumferential direction must be sufficient to provide the correct captured mass flow rate. The operability of HSCT inlet is mass flow rate sensitive. The error of the circumferential area representation should be sufficiently small so that it has no significant influence on the inlet operability. Figure 3 indicates that the circumferential mesh point is adequate because the pressure distributions predicted by the axisymmetric and three-dimensional mesh are almost identical.

Using the bisection root search iteration to find the proper back pressure corresponding to the critical operation is quite CPU intensive. The axisymmetric computation is much more efficient than the three-dimensional computation. Therefore, the second function of the axisymmetric computation is to help the three-dimensional computation search the back pressure corresponding to the critical

Table 1 Flow conditions

Parameter	Value
M_∞	2.0
$P_{t\infty}$	7.67×10^4 Pa
$T_{t\infty}$	390 K
Reynolds number	6.54×10^6/m
Bleed mass/captured mass	1.3%

Table 2 Grid parameters

Parameters	Three dimensional	Baseline axisymmetric	Refined axisymmetric
Grid points, streamwise	201	201	401
Grid points, radial	81	81	161
Grid points, circumferential	31	2	2
$\Delta x/\delta_{\text{throat}}$	0.3	0.3	0.15
$\Delta r^+_{1\,\text{max, centerbody}}$	2.3	2.3	0.98
$\Delta r^+_{1\,\text{av, centerbody}}$	1.3	1.3	0.6
$\Delta r^+_{1\,\text{max, cowl}}$	1.9	1.9	0.8
$\Delta r_{1\,\text{av, cowl}}$	1.1	1.1	0.5
Grid points within both BL_{throat}	33	33	65
Grid cells across bleed region	12	12	24

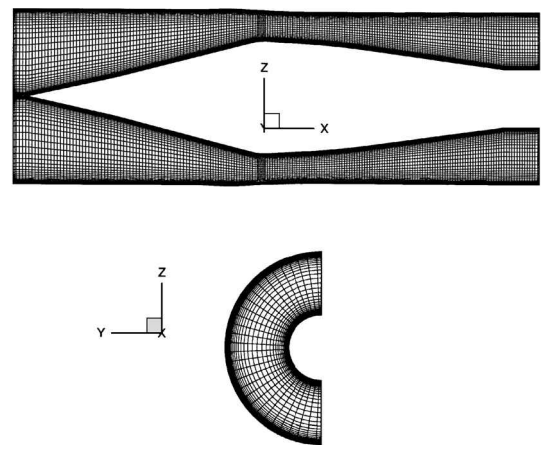

Fig. 2 Mesh of the mixed compression inlet: top, streamwise plane, and bottom, spanwise plane at the inlet exit.

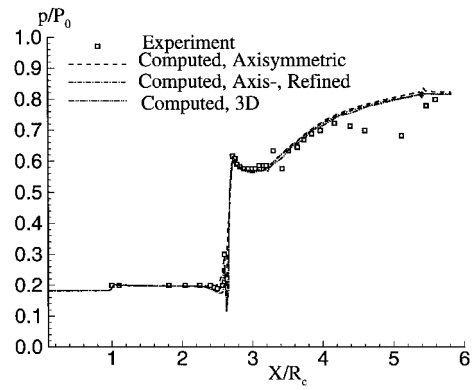

Fig. 3 Pressure distributions along the centerbody of the inlet for $M = 2.0$ at $\alpha = 0$ deg.

operation. The turnaround CPU time of the three-dimensional computation for one back pressure search varies from about 2 to 20 days on a single SGI Power Onyx R10000 processor corresponding to different back pressure values. We benefited from multiple (three) processors by submitting multiple jobs in parallel.

The bisection method was also used to search the unstart angle of attack. The turnaround CPU time for one search varies from 3 to 20 days on a SGI Power Onyx R10000 processor corresponding to different angles of attack.

B. Boundary Conditions

The upstream boundary conditions used fixed variables equal to those of freestream. The no-slip conditions were used for the solid wall. First-order extrapolation was used for the outer boundary upstream of the cowl leading edge. This boundary condition worked well to avoid the wave reflection, therefore omitting the computation of the outer zone of the inlet to save CPU time. At the subsonic outflow, the back pressure was held as constant on the whole inlet exit plane. All other variables were first-order extrapolated from the inner domain. These boundary conditions yield constant corrected mass flow rate during the process of varying the angle of attack, which is consistent with the experiment. However, the back pressure is a variable during the root search process using the bisection method to build up the critical operation. The back pressure was held constant within each iteration. Therefore, it is an accuracy assessment criterion to compare if the back pressure searched agrees well with the experiment.

The bleed boundary condition was first-order extrapolated for all of the variables except for the velocity component normal to the bleed region, which was determined based on a uniform bleed mass flow rate assumption. Assuming the local control volume i has the surface area a_i within the bleed region, if the total bleed area is A and total bleed mass flow rate is m_{bl}, then the velocity component V_{ni} that is normal to the bleed region is determined by

$$\rho_i V_{ni} a_i = (a_i/A) m_{\mathrm{bl}} \tag{1}$$

Thus,

$$V_{ni} = m_{\mathrm{bl}}/A\rho_i \tag{2}$$

The velocity component normal to the bleed region, therefore, is not uniform and varies with the density, which varies with the shock location and intensity. The total bleed mass flow rate was fixed in the computation. In the experiment, the total bleed mass flow rate with varying angle of attack was fairly constant due to the fixed bleed area and choked bleed strut valve. This bleed boundary condition may be extended to a variable bleed rate if the bleed flow coefficient can be accurately measured in an experiment. The tangential velocity component, as well as all other variables, were first-order extrapolated from the inner domain.

The physical arguments of this bleed boundary condition are as follows. 1) It gives the required bleed mass flow rate. 2) It simulates the flow going into a bleed slot with a large tangential velocity due to the flow expansion into the bleed slot. 3) It allows both the normal and tangential velocity profiles to vary with the shock location, structure, and intensity, which offers a certain flexibility for the shock wave to adjust itself within the bleed region. This boundary condition is a reasonable approximation to the slot bleed used in the experiment. Our numerical tests showed that this bleed boundary condition was robust and gave accurate shock location, structure, and intensity for the inlets simulated.

The current bleed boundary condition is similar to the boundary condition type 5 suggested by Chyu et al.[24] The difference is that we do not use the momentum equation to solve the pressure. We found that the momentum equation was not easily simplified and introduced numerical instability. In addition, we impose the first-order derivative of the tangential velocity to be zero, instead of the second-order derivative to be zero as in Ref. 24. The present bleed boundary condition was incorporated into the GASP code by the authors.

V. Mesh Refinement Computation

Mesh refinement is needed to assess the accuracy and uncertainty of the computation. As already mentioned, the three-dimensional computation is very expensive. The complete three-dimensional mesh refinement test is too CPU intensive to proceed, particularly due to the root search for the back pressure and the angle of attack. Therefore, we have to select a representative case to carry out the mesh refinement study.

As we mentioned earlier, we verified that the circumferential mesh size is sufficient by comparing the results with the axisymmetric case, as shown in Fig. 3. We believe that the same conclusion applies, even at angle of attack, because the angle of attack under investigation is not large, and hence, the flow variable gradient in the circumferential direction is far less than those in the streamwise and radial directions.

The case chosen for the mesh refinement study was the axisymmetric case with zero angle of attack. The mesh is refined in both the axial and radial directions. The refined mesh enhances the resolution of the wall boundary layer, oblique and normal shock wave system, and thus the shock wave/turbulent boundary-layer interaction. All of these physical phenomena are crucial in determining the inlet operability, i.e., start or unstart. If the result of the axisymmetric case with zero angle of attack is converged based on the mesh refinement, we are confident that the three-dimensional results of the baseline case will also be essentially grid independent in the inlet operability study.

Table 2 shows the grid resolution of the refined mesh with the size of 401×161 in the streamwise and radial directions, respectively. Figure 3 shows the pressure distribution (normalized by the freestream total pressure) computed using the baseline and refined meshes for the axisymmetric case with zero angle of attack. The abscissa is X/R_c, where R_c is the inlet cowl radius. The results are nearly identical. Figure 3 also indicates that the shock location and intensity predicted by the refined mesh is the same as that of the baseline case. The back pressure searched for the axisymmetric refined mesh to keep the inlet started at the critical operation is 0.17% lower than that of the axisymmetric baseline case. The back pressure difference of the three-dimensional and the refined axisymmetric computation is 0.4%. The mass-averaged total pressure recovery is predicted to be 0.945 for the axisymmetric refined mesh. The baseline axisymmetric case predicted the mass-averaged total pressure recovery to be 0.950, and the baseline three-dimensional case was predicted to be 0.939. The total pressure recovery of the refined mesh is in the middle of the results of the baseline axisymmetric and three-dimensional case, and the difference is within 0.7%. These results indicate that the mesh size of the baseline case is sufficient to resolve the boundary layer and shock waves.

VI. Results and Discussion

A. Zero Angle of Attack

The zero-angle-of-attack flow is used to initialize the flow computation at angle of attack. Detailed experimental results are also available to assess the accuracy of the computation.

Figure 3 shows the pressure distributions compared with the experiment[17] at zero angle of attack ($\alpha = 0.0$ deg) and critical operation. The experimental bleed mass rate of 1.3% is used. The back pressures searched from the axisymmetric and the three-dimensional cases deviate from the experiment by 2.5% and 1.8%, respectively, which is comparable to the experimental uncertainty. The shock location and intensity match the experiment very well. However, there is a pressure oscillation before the normal shock that is likely to be introduced numerically due to the shock interaction with the bleed boundary condition. It is obviously not due to the mesh resolution because both the baseline and refined mesh have the oscillation with about the same amplitude, as shown in Fig. 3. It is not clear if the oscillation could be attributed to the turbulence model used without some special tests. Nonetheless, this oscillation is acceptable and is a minor side effect compared with the overall good agreement of the shock location and shock intensity. The computed pressure also agrees very well with the experiment upstream and downstream of the shock.

There is a region downstream of $x/R_c = 4.2$ in the subsonic diffuser where the computation and experiment deviate. The reason is

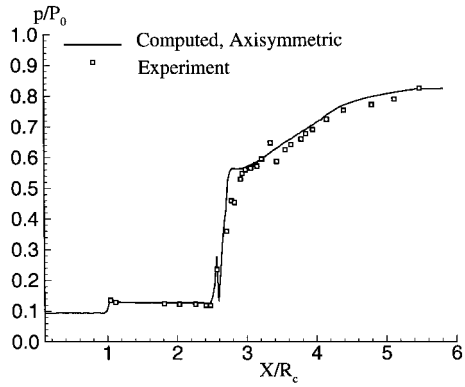

Fig. 4 Pressure distributions along the centerbody of the inlet for $M = 2.5$ at $\alpha = 0$ deg.

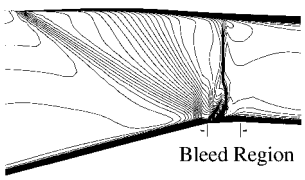

Fig. 5 Mach contours in the region of the throat at critical operation for $M = 2.0$ at $\alpha = 0$ deg.

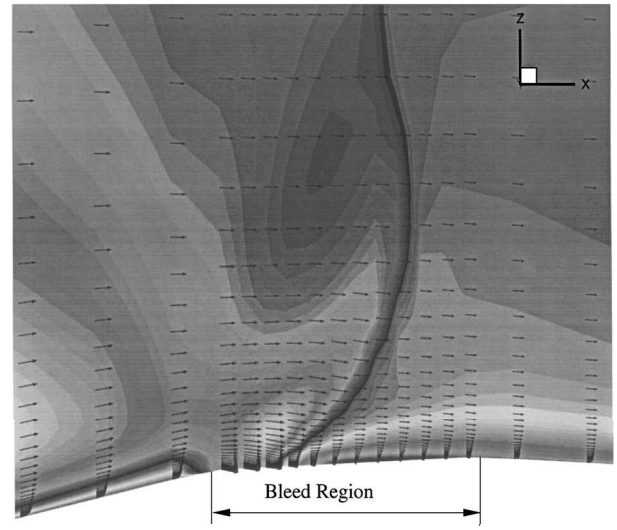

Fig. 6 Mach contours and velocity vector field in the bleed region for $M = 2.0$ at $\alpha = 0$ deg.

that the computation did not consider the four hollow centerbody support struts that were installed from about $x/R_c = 4.1$ to 5.6. This makes the area of the subsonic diffuser expand, then shrink, then expand, instead of monotonically increasing. Such area variation of the subsonic diffuser generated the pressure valley in the experiment. With no struts in the computation, the flow continuously decelerates to the inlet exit with no pressure drop. The experiment reported no flow separation, nor did our computation. Nonetheless, Fig. 3 indicates that the struts have little effect on the terminal shock position, which is important in this study.

To further verify the accuracy of the CFD code, in particular the boundary-layer bleed model, we computed the axisymmetric case at the inlet design point Mach 2.5, where the second cone angle (18 deg) is 3.5 deg higher than the Mach 2.0 case. Figure 4 displays the computational and experimental pressure distributions along the centerbody using the same mesh size as the baseline case. The shock location and intensity were again accurately predicted. The pressure distributions agreed very well in the subsonic diffuser without the deviation, as shown in the Mach 2.0 case, because the struts have less blockage area ratio in the Mach 2.5 case than in the Mach 2.0 case. The area of subsonic diffuser increased monotonically in the Mach 2.5 case. Also, neither the experiment nor the computation had separation in the flowfield for the Mach 2.5 case. The accurate prediction of the shock location, structure, and intensity supports the bleed boundary condition model used.

Figure 5 presents the Mach number contours of the three-dimensional computation at zero angle of attack in the region of the throat and shows the shock wave structure. An oblique shock generated by the cowl leading edge impinges upstream of the centerbody bleed. The normal terminal shock is located in the middle of the bleed region.

Figure 6 is the zoom of the bleed region with the Mach number contours and velocity vector field. The Mach number contours clearly show that the boundary-layer thickness upstream of the bleed region is increased due to the cowl shock wave impingement, and the slot bleed removes the boundary layer as desired. The velocity going into the bleed slot is large due to the expansion into the bleed slot and is abruptly reduced by the curved foot of the terminal shock wave standing in the bleed region. Downstream of the bleed region, the velocity profile quickly recovers to a normal shape with a thin boundary layer. This bleed flowfield structure has some similarity to what was observed by Shih et al.,[25] where the detailed flowfield in the bleed hole and plenum was simulated.

Figure 7 presents the total pressure profiles at the inlet throat ($X/R_c = 2.757$), throat exit ($X/R_c = 3.212$), and inlet exit ($X/R_c = 5.607$). The total pressure profiles reflect the boundary-layer shapes at those locations. At the inlet throat, which is immediately downstream of the inlet bleed region (the bleed region ends at $X/R_c = 2.722$), the boundary-layer profile computed on the centerbody agrees fairly well with the experiment (Fig. 7a). This shows, again, that the bleed boundary condition treatment is acceptable. At the throat exit (Fig. 7b), the boundary layer is thicker than at the throat. The computation, again, is in quite good agreement with the experiment. At the inlet exit (Fig. 7c), the computational total pressure profile does not match as well as at the throat exit. The reason for this outcome may be the following: 1) In the computation, there were no vortex generators as were used in the experiment to reduce the distortion by inhibiting flow separation; the vortex generators may affect the downstream total pressure profiles. 2) The computation did not simulate the struts, which may also have some influence on the total pressure distribution at the inlet exit. It is not known how much effect the turbulence model has in this case.

At Mach 2 and zero angle of attack, the computed mass-averaged total pressure recovery is 0.939 and the area-averaged total pressure recovery is 0.930. The experimental area-averaged total pressure recovery is 0.938. The computation deviates from the experiment only by 0.8% and is very accurate. This means that even though the total pressure profile is not precisely predicted at the inlet exit, the total pressure recovery as an averaged parameter, which is controlled by the energy conservation, can still be predicted accurately. However, the predicted steady-state distortion, according to the definition $d = (P_{t\max} - P_{t\min})/Pt_{\text{av}}$, is 0.167 and is significantly higher than the experimental value of 0.114. But the $P_{t\max}$ and $P_{t\min}$ were determined from the mesh points that were much more finely distributed than the experimental measurement probes on that cross section. To compare the accuracy of the computed distortion, we have to determine $P_{t\max}$ and $P_{t\min}$ from the same locations as those of the measurement probes. The computed distortion then becomes 0.128 and is still higher but is much closer to the experimental value of 0.114.

B. Prediction of Unstart Angle of Attack

After obtaining the flow at critical operation and zero angle of attack, computations of the flowfield with different angles of attack were performed with the same back pressure as that employed at zero angle of attack. In the experiment, the maximum angle of attack at which the inlet remained started at Mach 2 is 1.3 deg. In our computation, the inlet unstarted at the angle of attack of 1.6 deg and remained started at the angle of attack of 1.2 deg. Therefore, we take the angle of attack of 1.4 ± 0.2 deg as the maximum angle of attack at which the inlet can sustain at the critical operation without inlet unstart. The uncertainty of ± 0.2 deg falls within the experimental measurement uncertainty. The closer the angle of attack is to the maximum angle of attack for the inlet to remain started, the slower the terminal shock moves; therefore, more CPU time is required

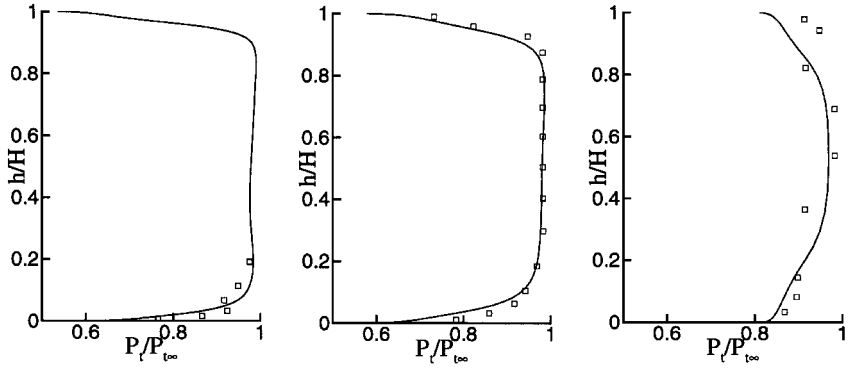

a) Throat $X/R_c = 2.757$ b) Throat exit $X/R_c = 3.212$ c) Inlet exit $X/R_c = 5.607$

Fig. 7 Total pressure profiles at zero angle of attack and at different axial locations: ——, computation, and □, experiment.

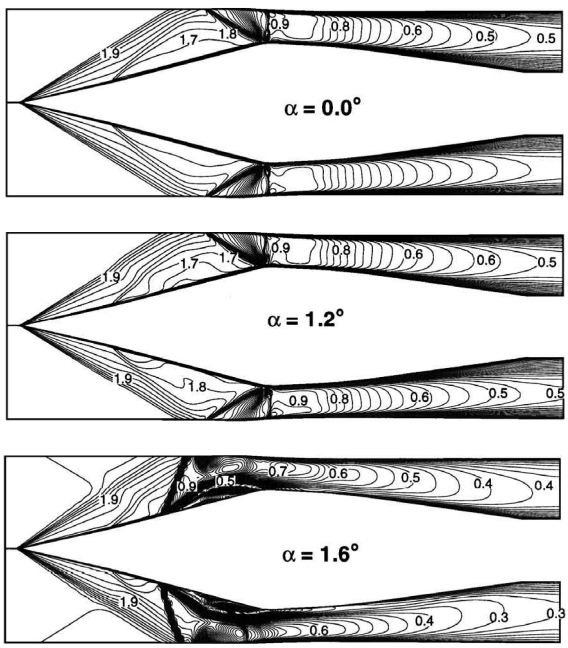

Fig. 8 Mach number contours at different angle of attack showing inlet started at $\alpha = 0$ and 1.2 deg and unstarted at $\alpha = 1.6$ deg.

to verify if the inlet will remain started or will eventually become unstarted. The CPU time increases dramatically with decreasing the uncertainty interval for the angle of attack.

Figure 8 shows the Mach number contours on the leeward and windward planes at different angles of attack. It is seen that the oblique shocks on the windward and leeward sides become asymmetric about the axis at angle of attack. The inlet remains started at angle of attack of 1.2 deg and becomes unstarted at angle of attack of 1.6 deg. Both solutions were converged. Figure 8 also shows that a large separation was induced by the bow shock in the forward portion of the inlet.

When the angle of attack varies from zero to 1.2 deg, Fig. 8 shows that the inlet exit Mach number remains about the same. Because the freestream thermal parameters, such as total temperature and total pressure, are the same during variation of angle of attack, the total temperatures computed at the inlet exit are virtually constant. The computed actual flow rate and total pressure at the inlet exit vary slightly at angle of attack compared with at zero angle of attack when the inlet remains started. But the corrected mass flow rates computed, which are determined by the actual flow rate, total temperature, and total pressure, remain constant during the process of varying angle of attack until the inlet unstarts.

The mechanism causing the inlet unstart due to angle of attack is analyzed in Ref. 26 using a time-accurate computation. It is briefly summarized as follows. When an angle of attack is imposed, the flow on the leeward side near the cowl leading edge has a stronger compression than that at zero angle of attack. The strong compression reduces the flow Mach number upstream of the terminal shock and, therefore, allows the shock move upstream first on the leeward side. When the terminal shock on the leeward side crosses the bleed region, it continues to travel upstream, and flow separation is induced on the shoulder of the inlet centerbody by the shock/boundary-layer interaction. The separation first occurs on the leeward side and then rapidly spreads to the whole inlet, resulting in the entire inlet unstart.

VII. Conclusions

A numerical simulation of NASA VDC HSCT inlet operability at angle of attack is successfully conducted. The extrapolation uniform mass bleed boundary condition suggested in this paper for the slot bleed is proven to be quite robust and accurate. The Baldwin–Lomax algebraic turbulence model performs favorably for the three-dimensional flow computation of the inlet. At zero angle of attack and Mach 2.0, critical operation flow is obtained with a back pressure that agrees with the experiment within 2.5%. The pressure distribution of the critical flow agrees very well with the experiment except for a portion of the subsonic diffuser where the inlet centerbody support struts were not simulated in the computation. The computed Mach 2.5 case with zero angle of attack was also in good agreement with the experiment. For both of the cases at zero angle of attack, the terminal shock location, intensity, and total pressure recovery all match closely with the experiment. For the Mach 2.0 case, the steady-state distortion on the compressor face is predicted higher than the experiment. The computed maximum angle of attack at which the inlet remains started is 1.4 ± 0.2 deg, which is in close agreement with the experimental value of 1.3 deg. The mesh refinement computation confirms that the solution is converged, based on the test for the axisymmetric flow with zero angle of attack.

Acknowledgments

This research is part of the Hypercomputing and Design (HPCD) project based at Rutgers University. The HPCD project is supported by the Defense Advanced Research Projects Agency of the Department of Defense through Contract ARPA-DABT 63-93-C-0064 monitored by Robert Lucas. United Technologies Research Center supported the efforts of Martin Haas under its Industrial Research and Development program. The authors would like to particularly thank J. D. Saunders at NASA Lewis Research Center for his helpful discussions and for providing his and other researchers' reference papers. Special thanks are also extended to G. C. Paynter at Boeing, Thomas I-P. Shih at Carnegie Mellon University, and J. W. Slater at the Institute for Computational Mechanics in Propulsion for their helpful discussions and for providing their research papers. The authors also greatly appreciate the help of William D. McGrory at Aerosoft, Inc., and Keith Miyake in the Department of Computer Science of Rutgers University to incorporate the bleed boundary condition subroutine into GASP code. We would also like to thank the *AIAA Journal* reviewers and editors for their comments.

References

[1]Committee on Aeronautical Technologies, *Aeronautical Technologies for the Twenty-First Century*, National Research Council, National Academy Press, Washington, DC, 1992.

[2]National Science and Technology Council, *Goals for a National Partnership in Aeronautics Research and Technology*, Executive Office of the President of the United States, Washington, DC, 1995.

[3]Saunders, J., and Keith, T., "Results from Computational Analysis of a Mixed Compression Supersonic Inlet," AIAA Paper 91-2581, June 1991.

[4]Hamed, A., and Lehnig, T., "An Investigation of Oblique Shock/Boundary Layer Bleed Interaction," AIAA Paper 90-1928, July 1990.

[5]Cooper, G., and Sirbaugh, J., "PARC Code: Theory and Usage," Arnold Engineering Development Center, AEDC-TR-89-15, Arnold AFB, TN, 1989.

[6]Slater, J. W., Chung, J., and Cole, G. L., "Computation of Unsteady Aeropropulsion Flows with Moving Geometry," *Proceedings of 1st Air Force Office of Scientific Research Conference on Dynamic Motion CFD*, Rutgers Univ., Piscataway, NJ, 1996, pp. 271–279.

[7]Mayer, D., and Paynter, G. C., "Prediction of Supersonic Inlet Unstart Caused by Freestream Disturbances," *AIAA Journal*, Vol. 33, No. 2, 1995, pp. 266–275.

[8]Mayer, D., and Paynter, G. C., "Boundary Conditions for Unsteady Supersonic Inlet Analyses," *AIAA Journal*, Vol. 32, No. 6, 1994, pp. 1200–1206.

[9]Slater, J. W., "Efficient Computation of Unsteady Planar Internal Viscous Flows with Moving Geometry," AIAA Paper 96-0113, Jan. 1996.

[10]Neaves, M. D., and McRae, D. S., "Numerical Investigations of Axisymmetric and Three-Dimensional Supersonic Inlet Flow Dynamics Using a Solution Adaptive Mesh," *Proceedings of 1st Air Force Office of Scientific Research Conference on Dynamic Motion CFD*, Rutgers Univ., Piscataway, NJ, 1996, pp. 235–243.

[11]Benson, R. A., and McRae, D. S., "A Three-Dimensional Dynamic Solution—Adaptive Mesh Algorithm," AIAA Paper 90-1566, 1990.

[12]Goble, B. D., King, S., Terry, J., and Schoop, M., "Inlet Hammershock Analysis Using a 3-D Unsteady Euler/Navier–Stokes Code," AIAA Paper 96-2547, July 1996.

[13]Miller, D. N., and Smith, B. R., "Time-Dependent CFD Analysis of Inlet Unstart," *Proceedings of 1st Air Force Office of Scientific Research Conference on Dynamic Motion CFD*, Rutgers Univ., Piscataway, NJ, 1996, pp. 291–297.

[14]Vadyak, J., Hoffman, J., and Bishop, A. R., "Calculation of the Flow Field in Supersonic Mixed-Compression Inlets at Angle of Attack Using the Three-Dimensional Method of Characteristics with Discrete Shock Wave Fitting," NASA CR-135425, 1978.

[15]Howlett, D. G., and Hunter, L., "A Study of a Supersonic Axisymmetric Spiked Inlet at Angle of Attack Using the 3-D Navier–Stokes Equations," AIAA Paper 86-0308, Jan. 1986.

[16]Bowditch, D. N., "Some Design Considerations for Supersonic Cruise Mixed Compression Inlets," NASA TM-X-71460, 1973.

[17]Wasserbauer, J. F., Shaw, R. J., and Neumann, H. E., "Design of a Very-Low-Bleed Mach 2.5 Mixed-Compression Inlet with 45 Percent Internal Contraction," NASA TM X-3135, March 1975.

[18]Wasserbauer, J. F., Neumann, H. E., and Shaw, R. J., "Distortion in a Full-Scale Bicone Inlet with Internal Focused Compression and 45 Percent Internal Contraction," NASA TM-X-3133, Dec. 1974.

[19]Wasserbauer, J. F., Neumann, H. E., and Shaw, R. J., "Performance and Surge Limits of a TF30-P-3 Turbofan Engine/Axisymmetric Mixed-Compression Inlet Propulsion System at Mach 2.5," NASA TP-2461, May 1985.

[20]Zha, G.-C., Smith, D., Schwabacher, M., Rasheed, K., Gelsey, A., and Knight, D., "High Performance Supersonic Missile Inlet Design Using Automated Optimization," *Journal of Aircraft*, Vol. 34, No. 6, 1997, pp. 697–705.

[21]"GASP v3 User's Manual," Aerosoft, Inc., May 1996.

[22]Mizukami, M., and Saunders, J., "Parametrics on 2D Navier–Stokes Analysis of a Mach 2.68 Bifurcated Rectangular Mixed-Compression Inlet," NASA TM-107003, July 1995.

[23]Zha, G.-C., Knight, D., Smith, D., and Haas, M., "Numerical Simulation of HSCT Inlet Operability with the Angle of Attack," AIAA Paper 97-2761, July 1997.

[24]Chyu, W., Howe, G., and Shih, T. I.-P., "Bleed Boundary Conditions for Numerically Simulated Mixed-Compression Supersonic Inlet Flow," *Journal of Propulsion and Power*, Vol. 8, No. 4, 1992, pp. 862–868.

[25]Shih, T. I.-P., Rimlinger, M., and Chyu, W., "Three-Dimensional Shock-Wave/Boundary-Layer Interactions with Bleed," *AIAA Journal*, Vol. 31, No. 10, 1993, pp. 1819–1826.

[26]Zha, G.-C., Knight, D., and Smith, D., "Numerical Investigations of HSCT Inlet Unstart Transient at Angle of Attack," AIAA Paper 98-3583, July 1998.

D. S. McRae
Associate Editor